Torregrosa, AJ.; De La Morena, J.; Sanchis Pacheco, EJ.; Redondo-Navarro, ÁR.; Servetto, E. (2022). A study of the early life of Gasoline Particulate Filters: reactive and dissipative acoustic effects. Proceedings of the Institution of Mechanical Engineers Part D Journal of Automobile Engineering. 1-11. https://doi.org/10.1177/09544070221127330

A study of the early life of Gasoline Particulate Filters: reactive and dissipative acoustic effects

A. J. Torregrosa[1], J. de la Morena[1], E. Sanchis[1], Á. Redondo[1] and E. Servetto[2]

[1]CMT - Motores Térmicos. Universitat Politècnica de València (Spain).
[2]PowerTech Engineering S.r.l. (Italy).

Corresponding author:
A. J. Torregrosa,CMT - Motores Térmicos. Universitat Politècnica de València (Spain). Campus de Vera, Edificio 6D. Camino de Vera s/n, 46022-Valencia, Spain.
Email: atorreg@mot.upv.es

Submitted to
Proceedings of the Institution of Mechanical Engineers Part D: Journal of Automobile Engineering

Abstract

The presence of after–treatment systems (ATS) has some side effects as they modify the wave dynamics, back–pressure and acoustic behavior of the exhaust system, that define the boundary conditions for the main silencing device. Gasoline particulate filters (GPF) have a considerable influence on these traits as their working principle depends on wall–flow monoliths; additionally, particulate filters have an inherent transient behavior due to the loading-regeneration cycles during their operation.

In this paper, the steady and unsteady behaviour of a typical device containing a three-way catalyst (TWC) and a GPF has been characterized in new (prior to any use) and used (after regeneration) conditions, with special focus on the role of dissipation. Pressure drop measurements were used in steady flow, whereas an acoustic energy balance was performed in the unsteady case that allows for the identification of the reactive and dissipative contributions.

The results obtained for the GPF suggest that it maintains a rather constant behaviour after it has been used for a relatively short time, to never reach back brand–new cleanness due to accumulation into the substrate pores, but remaining in an almost constant state over load–regeneration cycles burning the soot, and only suffering from ash accumulation over very long times. The results were then used to analyze the ability of a standard gas-dynamic code to reproduce the influence of the loading on the reactive and dissipative effects observed, with the main conclusion that by properly tuning the model parameters it is possible to reproduce, at least qualitatively, the trends observed in the experiments. The model can thus be used to provide adequate inlet conditions for the design of the exhaust line.

Keywords
Particulate Filter, Wall–Flow Monolith, After–treatment devices, Pressure Drop, Acoustic power balance

Introduction

The current trend to tighten emission regulations[1–3] is constantly pushing research and development efforts into improving engine performance and enhancing palliative after-treatment systems (ATS)[4–7]. To comply with those regulations, the exhaust line of vehicles using internal combustion engines has been gradually complicated by the presence of ATS.

The current state of diesel engine technology and the prominence of the gasoline direct injection (GDI) technology over other spark-ignited engine technologies have made that particulate matter (PM) has become a major issue in all automotive applications. The use of wall-flow particulate filters (PFs), namely Diesel particulate filters (DPF) for all Diesel vehicles and gasoline particulate filters (GPF) for GDI vehicles[8–11], has become the standard and most reliable approach to abate PM emissions; both technologies usually consist of filters with honeycomb structure made of extruded porous ceramic materials as the substrate, with or without different catalytic washcoats, and with a similar cell density, through which the exhaust gases are forced to flow, trapping the PM in the process.

The DPF technology can be traced back to the late 1970's, when it was known as Particulate Trap[12,13], but the less strict emission regulations, together with continuous advances in Diesel engine design, calibration

and specific technological improvements allowed Diesel engines to avoid or minimize the use of DPF until the late 2000's, when it became standard. On the other hand, the GPF is much more recent, increasing in number alongside GDI engines, which have gained most of the market in new gasoline-fueled vehicles due to better torque and power output, fuel economy and dynamic driving responsiveness[14,15]. Similarly to what happened with diesel engines, advances in GDI engines such as improvements of combustion technology may help to reduce PM emission, but with the current real driving emission test, enforced in 2017, the GPF has also become standard[16].

In GPF development it has been attempted to transfer DPF knowledge and working principles into GDI engines; however, even though some knowledge gained in the development and application of DPFs can be successfully transferred, aspects such as PM composition, mass to number ratio, exhaust gas temperature and composition from gasoline engines are significantly different from those found in Diesel engines[17] and thus need its own research. It is worth noting that the particle size of the GDI emissions is relatively small, mostly less than 100 nm in diameter, in very large quantities but representing only a small fraction of the mass. This kind of particles are a serious threat to air quality and human health, as they are directly related to an increased risk of respiratory diseases[18].

The complete cycle of operation of a PF, either DPF or GPF, consist of a continuous succession of loading and cleaning processes; even though specific characteristics of each process vary, the overall principles are essentially the same. Both kinds of filter are made of materials specifically designed to hold a certain quantity of PM, and during the loading process the accumulation of PM slowly creates a restriction to the flow, increasing the pressure drop across the filter, which could eventually result in clogging of the filter and have a negative impact on engine operation[12,19,20]. Therefore, PF systems need a cleaning process to remove

trapped PM and rehabilitate their soot collection capacity so that proper engine operation is guaranteed. In that process, called regeneration, the trapped soot is incinerated, and the process can occur discretely when a certain quantity of soot has been captured, or continuously over regular operation[19–21].

In the loading process, two internal phenomena occur simultaneously: soot accumulation and ash accumulation. Soot accumulation occurs over short periods, within the time scale of a few hours, and ends with the regeneration process. However, not all the trapped material is burned, as a small amount of inorganic ash is left behind each time, which in turn accumulates over much longer time scales, typically of the order of several thousand hours, due to the small amount contained in the soot which is in the range of 0,5% to 1,0%[22]. The accumulated ash is immune to regeneration, therefore poisoning and deteriorating the PF useful life, while also impacting fuel-economy and potentially complicating on-board control[23]. Both soot and ash accumulation increase backpressure within their own time scales, compromising and modifying efficiency, acoustics and gaseous emissions.

Two main different mechanisms of soot filtration may be distinguished during the loading process. First, particle deposition fills material pores changing the substrate microstructure. This initial mechanism is called "deep–bed" filtration[24] and causes a steep increase in pressure drop[25]. Later, as all the available space within the substrate pores is filled, particles begin to agglomerate on top of the channel walls, leading to the formation of a continuous and consistent layer, which is called soot cake, and accordingly the mechanism is known as "soot cake" filtration; this is accompanied by a modest pressure drop increase, when compared to the previous mechanism, and almost 100% filtration efficiency[25,26]. Most of the soot captured resides in the soot cake layers[27,28]. The much slower and regeneration-immune ash particles that are trapped can be found in one

or both of the following forms: as an ash layer on top of the filter walls or as a more compact plug at the closed end of the channels. A simplified representations of the different ash and soot formation processes described can be seen in Figure 1.

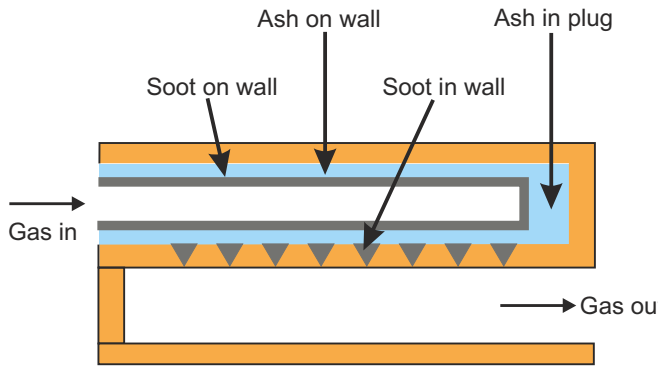

Figure 1. Schematic of a wall-flow particulate-filter, adapted from [27].

Once accumulation during the loading process has reached a certain level, the regeneration process takes place, and trapped soot particles are oxidized either by O_2 or NO_2 for sufficiently h igh temperatures, producing a variety of gaseous products, being CO_2 that most abundant. If all the required conditions are fulfilled n aturally d uring operation, either continuously as in GPF, or discretely as in some DPF, the process is called Passive Regeneration; on the contrary, if additional auxiliary systems are used to propitiate the regeneration it is called Active Regeneration[12,29], this latter also entailing some fuel consumption penalty, which is around 2%-3% extra fuel consumption, while passive regeneration strategies can drop this penalty by about 80%[30]. A proper performance of the regeneration mechanism sustains a stable cycle of soot capture and oxidation in the filter[29,31]. S everal o peration conditions determine filter r egeneration p erformance, t emperature b eing t he most important[32], followed by the soot load in the filter.

As there are similarities between DPFs and GPFs, there are also differences, both in engine operation and in the filter devices themselves. For instance, Diesel engines run on excess of oxygen, whereas gasoline engines run with closer to stoichiometric mixtures, thus changing the availability of air in the exhaust, which in turns facilitates or complicates the conditions for regeneration. The higher temperatures allow for frequent, almost continuous regeneration in GDI engines, whereas in diesel engines additional adjustments are needed, either increasing exhaust gas temperature or lowering the soot ignition temperature via the inclusion of a catalyst. Thermal passive regeneration is undoubtedly the cleanest and most attractive method for regenerating DPFs[12,31].

Compared to DPFs, GPFs are generally exposed to higher exhaust temperatures, lower oxygen concentrations, and fewer particles. Regeneration for GPFs is always passive, whereas DPFs can use either passive or active mechanisms. GPFs have higher porosity, which while allows the gas to move more easily across the substrate, also compromises mechanical properties since the substrate is lighter and hence more fragile. The average capacity of a DPF is around 8 grams of soot per liter (g/l), whereas for a GPF the average capacity is around 1 g/l. The reduced storage capacity of GPFs is not as problematic as it could seem, as gasoline particulate emissions are about 10 to 30 times smaller, and the frequent regeneration makes it difficult to form and maintain a cake layer on the substrate wall[33].

There are some studies in the literature on the early service life of GPFs[7,33,34], whose results suggest that at this stage, filtration performance is strongly affected by mass deposition and depends on the microstructure of the substrate: due to their reduced size, GDI particles are capable of entering the porous walls, modifying the overall substrate structure and therefore the filtration performance.

The effects of all these characteristics on exhaust wave dynamics arise in two different ways: *reactive* effects, mostly associated with wave reflection at the device, and *dissipative* effects associated with flow losses. Such effects determine the wave pattern in the exhaust line downstream of the ATS, and thus set the attenuation required from the silencer. The usual approach is to consider what would be the worst scenario, that is, the device in "new" condition. However, the fact that this condition may not be found in practice introduces an unnecessary complication in the design of the exhaust line. In fact, the dissipative effects of usage will in general reduce wave transmission across the ATS, thus reducing the actual noise source at the outlet, whereas the reactive effects will contribute to the reduce the negative impact of any resonances associated with the duct connecting the ATS and the muffler. Therefore, with some proper assessment of the influence of usage on the reactive and dissipative behaviour of an ATS including a GPF, design requirements could be relaxed and the development time and costs reduced.

Consequently, in this work the focus has been put on the comparison of "new" and "used" conditions. The former refers to the never-used state (the devices used were supplied directly from the factory, even with the catalyst bricks sealed), whereas the latter corresponds to the base state acquired by the particulate filter after the device has been used, loaded, and regenerated, but for a short time and distance, in order to avoid that any significant amount of ash may enter the filter. This condition is comparable to that of a vehicle particulate filter at the moment of reaching the customer in a new car, and the very first uses.

The paper is organized as follows: first, the different magnitudes used for the analysis of dissipative effects will be briefly described alongside the experimental procedures used, and some basic data of the device used will be provided. Then, the results obtained both from the experiments and from a standard commercial gas-dynamic code will be discussed and

analyzed, both from the point of view of the reactive and dissipative effects observed in the experiments, and from the point of view of the ability of the model to reproduce such effects. Finally, the main conclusions of the work will be summarized.

Assessment of reactive and dissipative effects

Two flow configurations were considered to analyze the effects of dissipation: steady flow and impulsive flow. The steady flow, apart from being consistent with the usual practical criteria, provides a good approximation to real exhaust flows at high engine speed, where the mean component clearly dominates over any fluctuation induced by engine operation[35]. The impulsive flow provides information also on the dynamic response of the devices, that dominates in low to medium engine speeds, and thus on the influence of dissipation on that response.

In the steady flow configuration, the total pressure drop across the ATS was measured as a function of the mass flow rate for mass flows up to 0.22 kg/s and in cold conditions (ambient temperature) as, even if the temperatures in the real exhaust are considerable, it has been demonstrated[36] that cold flow results may be soundly extrapolated to hot conditions. The details of the experimental procedure, which makes use of two measurements (one for the ducting alone and the other including the ATS) can be found in reference[37]. These results were then processed in order to obtain the pressure drop coefficient (i.e. the ratio of the total pressure drop to the upstream kinetic energy) as a function of the Reynolds number (Re). Both magnitudes provide a preliminary assessment of the influence of soot deposition on the dissipative behaviour of the ATS.

In the case where impulsive flow is used, the acoustic power balance provides a direct and complete picture of the unsteady behaviour of the ATS. Consider an after-treatment device, subject to an upstream excitation and with an anechoic (non-reflecting) termination at the downstream side

(this is the actual situation in the experimental setup used; details can be found in reference[38]), as shown in Figure 2.

Figure 2. The after-treatment system subject to an upstream excitation and with a non-reflecting downstream termination.

The power balance may be expressed by stating that the difference between the acoustic power upstream of the device and that downstream is the power dissipated at the device. This can be expressed as

$$W_i = W_r + W_t + W_d \tag{1}$$

where W_i is the acoustic power incident on the device, W_r is the power reflected, W_t is the power transmitted downstream and W_d is the power dissipated in the device. Of course, the value of W_d is actually obtained from equation (1). Expressions for the other terms are[39]:

$$W_i = \frac{S_1}{\rho c} \left|P_1^+\right|^2 (1 + M_1)^2 \tag{2}$$

$$W_r = \frac{S_1}{\rho c} \left|P_1^-\right|^2 (1 - M_1)^2 \tag{3}$$

$$W_t = \frac{S_2}{\rho c} \left|P_2^+\right|^2 (1 + M_2)^2 \tag{4}$$

where P_1^+ and P_1^- are the spectra of the forward and backwards wave components upstream of the device, respectively, and P_2^+ is the spectrum of the forward wave component transmitted downstream of the device (as the termination is anechoic, for the corresponding backward component

one has $P_2^- = 0$); S represents the cross-sectional area, ρ is the density, c is the speed of sound and M is the Mach number.

In order to identify the contributions of reactive and dissipative effects, one may consider that any reflection from the device is substantially determined by reactive effects, and therefore these can be characterized by the reflected power ratio W_r/W_i. From equations (2) and (3), one obtains that the reflected power ratio is

$$\frac{W_r}{W_i} = \frac{\left|P_1^-\right|^2}{\left|P_1^+\right|^2}\frac{(1-M_1)^2}{(1+M_1)^2} = \frac{(1-M_1)^2}{(1+M_1)^2}\left|R\right|^2 \tag{5}$$

where $R = P_1^-/P_1^+$ is the reflection coefficient of the system, that is a direct result of the experimental method used[38].

Then, the power that is not reflected back is either dissipated or transmitted, and thus the proper way to characterize dissipation appears to be the ratio of the power dissipated to the power not reflected, i.e. $W_d/(W_i - W_r)$, that will be referred to as dissipated power ratio. From equations (1) to (4) one gets

$$\frac{W_d}{W_i - W_r} = 1 - \frac{S_2}{S_1}\frac{\left|P_2^+\right|^2(1+M_2)^2}{\left|P_1^+\right|^2(1+M_1)^2 - \left|P_1^-\right|^2(1-M_1)^2} \tag{6}$$

and introducing the transmission coefficient of the system, $T = P_2^+/P_1^+$, again a direct result of the experimental method, one finally has

$$\frac{W_d}{W_i - W_r} = 1 - \frac{S_2}{S_1}\frac{\left|T\right|^2(1+M_2)^2}{(1+M_1)^2 - \left|R\right|^2(1-M_1)^2} \tag{7}$$

These two power ratios form the basis of all the subsequent analyses performed.

Studied device

The device considered is depicted in figure 3; it is a standard production part representative of current practice. Relevant geometrical data for the monoliths is given in Table 1.

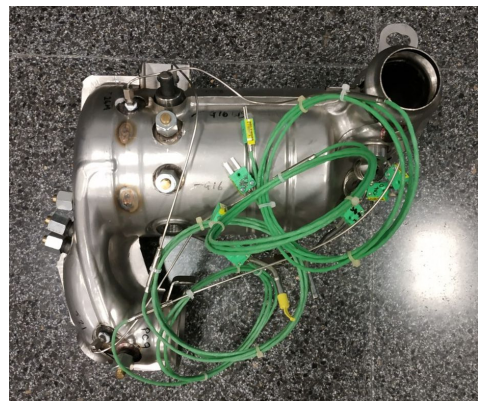

Figure 3. Device studied.

Table 1. Characteristics of the Monoliths in the device studied.

Characteristic	TWC Monolith	GPF Monolith
Length [mm]	45	118.1
Diameter [mm]	118.4	118.4
Monolith volume [l]	0.33139	1.13263
Cell size [mm]	1.037264 (estimated)	1.263518
Wall thickness [mm]	0.0889	0.2032
Cell density [cpsi]	600	150 (open) 300 (total)
Number of channels [#]	10239	2559 (open) 5118 (total)
Porosity [%]	-	50% (assumed)

After the device in new condition was measured for pressure drop and acoustics, a series of 10 WLTP cycles, equivalent to 232.5 km of road distance or 5 hours of driving time, and with the specific g ear shifts configured for a Sport Utility Vehicle, was performed during a complete

day on the native engine of the system. The device was instrumented to obtain the evolution of the pressure differential across the system, in order to evaluate the evolution of GPF loading along the test. The results obtained are shown in figure 4, where for clarity only the first, the fifth and the last two cycles are represented.

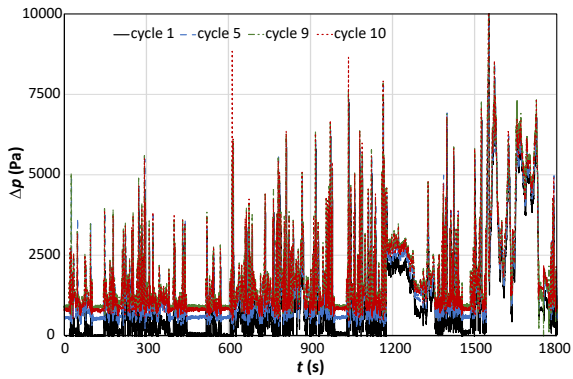

Figure 4. Evolution of the pressure differential across the system.

It can be observed that, while the pressure differential increases from cycle 1 to cycle 5, and from cycle 5 to cycle 9, the results for cycle 10 are almost indistinguishable from those of cycle 9, and even a little smaller. This should indicate that, at this point, passive regeneration has taken place but, as commented in the introduction, the system does not retrieve its initial condition but reaches its effective base state related with deep-bed filtration. In order to obtain a proper perspective of the system evolution, the integral of the pressure drop over each cycle was computed, and the results were normalized by the maximum value. The results are shown in figure 5.

As indicated by the tendency line included, there is a reasonable growing trend up to cycle 9, whereas for cycle 10 a noticeable decrease is observed, that should correspond to the onset of the passive regeneration. It was thus concluded that the state achieved by the system

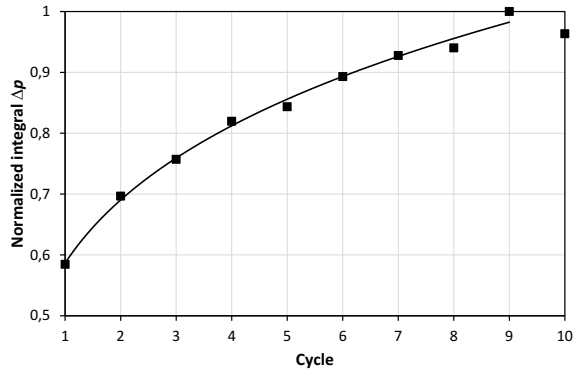

Figure 5. Evolution of the normalized integral of the pressure differential for the ten cycles.

is representative of the used condition, i.e. the actual state of interest for the present work.

Once these engine tests were performed, the device was measured again for pressure drop and acoustics so that its behaviour in used condition could be assessed.

Results: pressure drop

In figure 6 the effect of the usage on the pressure drop of the device studied is shown. It is apparent that, as expected, the pressure drop of the used device is only slightly higher than that of the new one. In both cases, the dependence of pressure drop on the mass flow is essentially quadratic, but with a non-negligible linear contribution, associated with the existence of laminar flow in the TWC and, most notably, across the wall-flow filter[36].

The modelling work was performed with GT-Power, that was used to emulate in full the experimental procedure. The basic approach consisted in tuning the model parameters so that the best possible reproduction of the results of the experiments in "new" condition was achieved, and then introduce a physically meaningful modification (namely, a reduction in the substrate pore diameter that could mimick the effects of deposition)

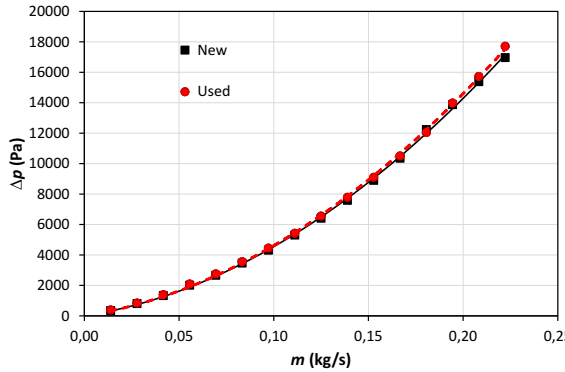

Figure 6. Experimental steady analysis: pressure drop.

so that the results of the experiments in "used" conditions could also be reproduced. The results are shown in figure 7, where it is apparent that, while the experimental trend observed in figure 6 is qualitatively reproduced, the values at maximum mass flow rate are slightly smaller than the experimental ones, and the influence of usage is more apparent. This is due to the fact that, with the tuning parameters available, it was not possible to reproduce in full the actual dependence of any of the devices, but only to produce results that exhibited acceptable errors throughout the mass flow range considered, so that the model slightly overestimates the pressure drop at moderate mass flows with a corresponding underestimation at high mass flows. This might indicate that the fact that the loading is not uniform across the wall-flow filter is not negligible, even for an integrated magnitude as the pressure drop.

Results: unsteady behaviour

Following the discussion on the acoustic power balance, the effect of usage on the reflected power ratio W_r/W_i is shown in figure 8.

One can observe that there is a noticeable influence of the usage on the reactive behaviour of the system: while the overall trends in terms of

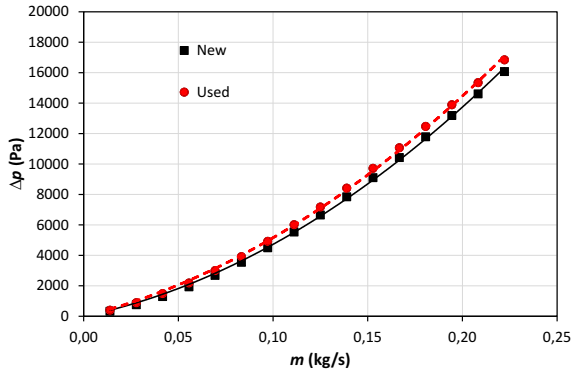

Figure 7. Modelling steady analysis: pressure drop.

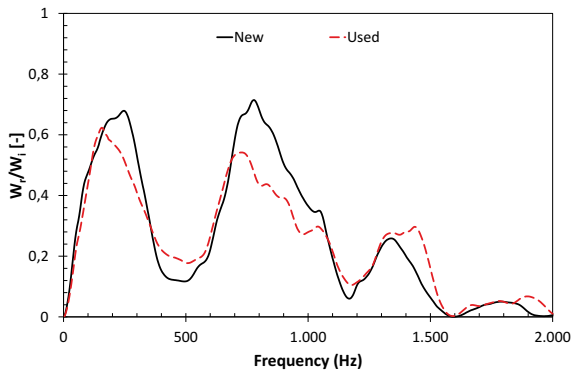

Figure 8. Unsteady experimental results: influence of the usage on the reflected power ratio.

the frequencies associated with peaks and troughs are not affected, the results corresponding to the used case exhibit in general less pronounced fluctuations up to frequencies around 1200 Hz. Above this frequency, the usage gives rise to an increase in the reflected power ratio that causes that its value is always close of above that corresponding to the new condition. Such an effect should be related with the fact that relatively high frequencies are more affected by geometrical changes at the substrate level.

Regarding the modelling results, these were obtained by simulating an acoustic rig with GT-Power, making use of the same model parameters as in the steady computation. From the transfer matrix so obtained, it was possible to compute the transmission and reflection coefficients and thus the two power ratios used in the analysis. The results obtained for the reflected power ratio are shown in figure 9.

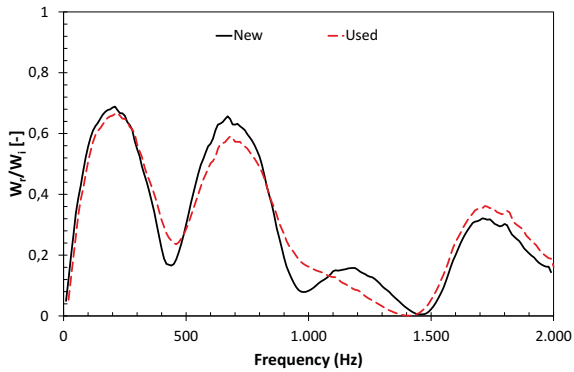

Figure 9. Unsteady modelled results: influence of the usage on the reflected power ratio.

Two main aspects of these results should be commented. First, the overall shape of the frequency dependence of the reflected power ratio is essentially captured for frequencies below 1000 Hz (consistently with the claims of the software developer) and, even above that frequency, certain aspects are reproduced. In fact, the values attained at the two highest peaks are quite close to those found in the experiments. However, it is also clear that the model is not able to fully reproduce the precise shape found in the experiments.

Secondly, the model is able to reproduce qualitatively the influence of usage, but the effect is less pronounced than that observed in the experimental results. Even so, the frequency distribution of those effects matches quite closely the experimental one (except between 1000 and 1500 Hz) and even the fact that the used device is more reflective at high

frequencies is reproduced. This indicates that, from the point of view of reactive mechanisms, the model is able to provide significant results.

The effect of usage on the experimental dissipated power ratio $W_d/(W_i - W_r)$ is shown in figure 10. It can be observed that for frequencies above 1000 Hz differences are relatively small, and regardless of the usage the attenuation produced by the system is essentially dominated by dissipation. The effect of usage is however apparent for frequencies below 1000 Hz: it can be seen that usage smooths out the curve, most notably at the two frequencies at which the main spikes of the reflected power ratio occur. Overall, as expected, dissipation is higher in used conditions, what can be an advantage when designing the eventual downstream silencer, as pointed out in the introduction.

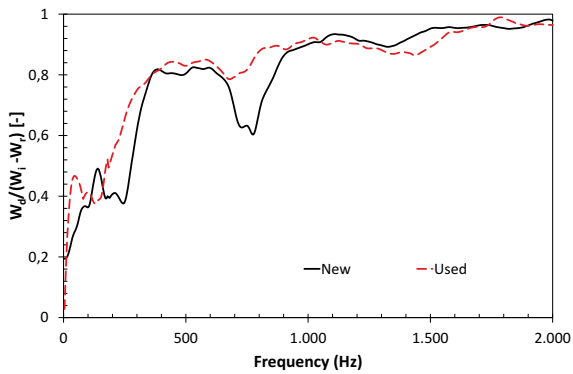

Figure 10. Unsteady experimental results: influence of the usage on dissipated power ratio.

When considering the corresponding modelled results, shown in figure 11, it is apparent that while the model was able to reproduce, at least qualitatively, the trends observed in the reflected p ower ratio, in this case a rather poor description of the dissipative behaviour is achieved, most notably in the case of the new condition, where a much smoother behaviour than that found in the experiments can be observed. Additionally, the effect of usage seems to be an almost constant increase

with respect to the new condition, without any of the frequency-dependent features observed in the experiments. This is fully consistent with the comments made regarding the effect of usage on the pressure drop, in the sense that the non-uniform distribution of the loading across the wall-flow filter has a significant impact on the dissipation, that is still more evident when unsteady results are analyzed.

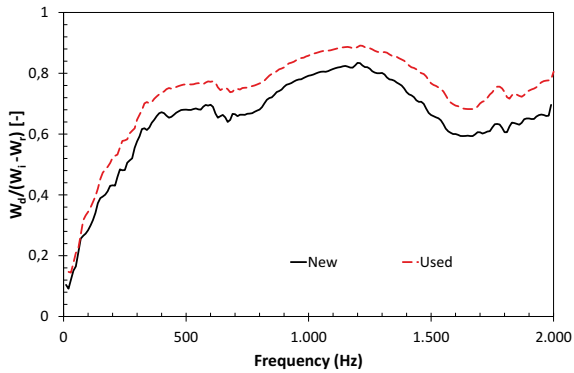

Figure 11. Unsteady modelled results: influence of the usage on dissipated power ratio.

Summary and conclusions

The opportunity to have access to an ATS representative of commercial use (TWC-GPF), directly from the factory, allowed to assess the differences between the "new" and the "used" conditions, i.e., the early life of the device, while trying to identify the role of reactive and dissipative effects on wave propagation, as they may contribute significantly to important simplifications in the design of the exhaust line downstream of the ATS.

The study was mainly focused on the effects of the first few cycles in the PF element, as it is known to undergo a deep-bed filtration which partially fills substrate pores and is in practice immune to regeneration, thus defining the effective base substrate microstructure and cleanness of

the wall-flow monolith and of the whole system. The facilities and testing methodologies used allowed to characterize the steady flow behaviour through pressure drop measurements and the unsteady flow behaviour through measurements in impulsive flow, both before and after undergoing 10 WLTP cycles in order to represent the first few cycles, while keeping any effect of ash accumulation at a minimum (equivalent to 232.5 km of road distance and about 5 hours through different engine regimes).

Aside of the experimental characterization, a standard gas-dynamic code was used to replicate experiments and analyze its ability to reproduce the differences found between the new and used conditions. Overall results indicate that, with a proper tuning of the model parameters, indicative values and trends are reproduced, at least qualitatively, for most of the frequency range studied.

The steady flow results showed hints of the influence of in-pore soot deposition on the dissipative behaviour of the ATS. The pressure drop of the device increased slightly with the use. The substrate pore diameter was the model parameter chosen to represent the deep-bed filtration in used condition, keeping the rest of the model parameters at the same value as for the new condition. For both conditions qualitatively good results were obtained, with a tendency to slightly overestimate at low to mid mass flows, and underestimate at high mass flows, the pressure drop. As the influence of usage is also more apparent in the modeled results, all this might indicate that the effect of load distribution across the wall-flow filter may have a noticeable influence on the overall pressure drop.

For the unsteady behaviour, two power ratios (reflected and dissipated) were used to highlight the relative importance of reactive and dissipative effects, both in the experimental and in the modelled results. In the case of the reflective/reactive contribution, the main conclusions drawn from the experiments were:

- The effect of usage showed noticeable influence on the reactive behaviour of the ATS.
- Overall trends were maintained in terms of peaks and troughs, with the used condition showing less pronounced fluctuations up to 1200 Hz, and quite close to new condition above that frequency, which can be related to higher frequencies being more sensitive to geometrical traits than to microstructure.

From the modelling work the following points are worth mentioning;

- The models are able to capture the overall shape of the frequency dependence (if not its details) for frequencies below 1000 Hz, as well as some other aspects above that value. Additionally, the values of the two highest peaks are quite close to their experimental counterparts.
- The model was able to reproduce qualitatively the effects of usage, showing that the "used" condition is more reflective at high frequencies. Even if the effect is less pronounced than that observed in the experiments, it can be stated that the model provides significant results from the point of view of reactive mechanisms.

In the case of the dissipative contribution, the main experimental outcomes were:

- The effect of usage induces relatively small differences for frequencies above 1000 Hz, and regardless of the usage effect, the attenuation is dominated by dissipative effects.
- The usage smooths out the curve for frequencies below 1000 Hz, most notably at the frequencies at the peaks of the reflected power ratio.
- Overall, dissipation is higher in used conditions, as one could expect.

From the modelling results, one may conclude that:

- The description of the dissipative behaviour provided by the model was rather poor, most notably in the case of the new condition, where results are much smoother than the experimental ones.
- The effect of usage is represented by an almost constant increase in dissipation in comparison with the new condition, therefore not accounting for any of the frequency-dependent features observed in the experiments. This is fully consistent with the comments pointed out when discussing the effect of usage on the pressure drop, thus supporting the assumption that the non-uniform distribution of the loading across the wall-flow filter has a significant impact on the dissipation, which is still more noticeable in unsteady conditions.

As an overall conclusion, it appears that accounting for these effects, even if approximately, may provide significant advantages from the point of view of exhaust line design.

Acknowledgements

The authors wish to thank A. Guzmán for his assistance with the experiments, and F. Morin and A. Bianco for many fruitful exchanges.

Declaration of conflicting interests

The authors declare no potential conflicts of interest with respect to the research, authorship, and/or publication of this article.

Funding

Álvaro Redondo is supported by Universitat Politècnica de València through the Programa de Ayudas de Investigación y Desarrollo [PAID–01–19] which grants his predoctoral contract.

Nomenclature

c	speed of sound	[m s^{-1}]
$\dot{m}$	mass flow rate	[kg s^{-1}]
M	Mach number	[–]
p	pressure	[Pa]
P	pressure spectrum	[Pa]
Re	Reynolds number	[–]
S	cross-sectional area . . .	[m^2]
W	Acoustic power	[W]

Greek symbols

ρ	mass density	[kg m^{-3}]

Superscripts

$+$	forward
$-$	backward

Subscripts

i	incident
r	reflected
t	transmitted
d	dissipated

Acronyms

ATS	After–Treatment System
DPF	Diesel Particulate Filter
GDI	Gasoline Direct Injection
GPF	Gasoline Particulate Filter
PF	Particulate Filter
PM	Particulate Matter
TWC	Three–Way Catalyst
WLTC	World Harmonized Light-duty Vehicle Test Procedure

References

1. Jiaqiang E, Zhao X, Qiu L et al. Experimental investigation on performance and economy characteristics of a diesel engine with variable nozzle turbocharger and its application in urban bus. *Energy Conversion and Management* 2019; 193: 149–161.
2. Meng Z, Chen C, Li J et al. Particle emission characteristics of dpf regeneration from dpf regeneration bench and diesel engine bench measurements. *Fuel* 2020; 262: 116589.
3. Zhong W, Tamilselvan P, Wang Q et al. Experimental study of spray characteristics of diesel/hydrogenated catalytic biodiesel blended fuels under inert and reacting conditions. *Energy* 2018; 153: 349–358.
4. Ogata T, Makino M, Aoki T et al. Particle number emission reduction for gdi engines with gasoline particulate filters. Technical report, SAE Technical Paper, 2017.
5. Qian Y, Wu Z, Guo J et al. Experimental studies on the key parameters controlling the combustion and emission in premixed charge compression ignition concept based on diesel surrogates. *Applied Energy* 2019; 235: 233–246.
6. Jiaqiang E, Zhao M, Zuo Q et al. Effects analysis on diesel soot continuous regeneration performance of a rotary microwave-assisted regeneration diesel particulate filter. *Fuel* 2020; 260: 116353.
7. Li Z, Shen B, Zhang Y et al. Simulation of deep-bed filtration of a gasoline particulate filter with inhomogeneous wall structure under different particle size distributions. *International Journal of Engine Research* 2021; : 1468087421992216.
8. Serhan N, Tsolakis A and Martos F. Effect of propylene glycol ether fuelling on the different physico-chemical properties of the emitted particulate matters: Implications of the soot reactivity. *Fuel* 2018; 219: 1–11.

9. Lee J, Lee S and Lee S. Experimental investigation on the performance and emissions characteristics of ethanol/diesel dual-fuel combustion. *Fuel* 2018; 220: 72–79.
10. Nabi MN and Rasul M. Influence of second generation biodiesel on engine performance, emissions, energy and exergy parameters. *Energy conversion and management* 2018; 169: 326–333.
11. Jiang C, Li Z, Qian Y et al. Influences of fuel injection strategies on combustion performance and regular/irregular emissions in a turbocharged gasoline direct injection engine: Commercial gasoline versus multi-components gasoline surrogates. *Energy* 2018; 157: 173–187.
12. Khair MK. A review of diesel particulate filter technologies. Technical Report 2003–01–2303, SAE Technical Paper, 2003.
13. Seizinger D. Analysis of carbonaceous diesel emissions. *UNIV RSI* 1979; : 216–220.
14. Saito C, Nakatani T, Miyairi Y et al. New particulate filter concept to reduce particle number emissions. Technical report, SAE Technical Paper, 2011.
15. Chan TW, Meloche E, Kubsh J et al. Evaluation of a gasoline particulate filter to reduce particle emissions from a gasoline direct injection vehicle. *SAE International Journal of Fuels and Lubricants* 2012; 5(3): 1277–1290.
16. Masumitsu N, Otsuka S, Fujikura R et al. Analysis of the pressure drop increase mechanism by ash accumulated of coated gpf. Technical Report 2019–01–0981, SAE Technical Paper, 2019.
17. Rubino L, Thier D, Schumann T et al. Fundamental study of gpf performance on soot and ash accumulation over artemis urban and motorway cycles-comparison of engine bench results with gpf durability study on road. Technical Report 2017–24–0127, SAE Technical Paper, 2017.
18. Myung C and Park S. Exhaust nanoparticle emissions from internal combustion engines: A review. *International Journal of Automotive Technology* 2012; 13(1): 9.
19. Ootake M, Kondou T, Ikeda M et al. Development of diesel engine system with dpf for the european market. Technical report, SAE Technical Paper, 2007.
20. Mikulic I, Zhan R and Eakle S. Dependence of fuel consumption on engine backpressure generated by a dpf. Technical report, SAE Technical Paper, 2010.
21. Bromberg L, Cohn DR and Wong V. Regeneration of diesel particulate filters with hydrogen rich gas. Technical report, MIT Plasma Science and Fusion Center, 2005.
22. Sappok AG and Wong VW. Detailed chemical and physical characterization of ash species in diesel exhaust entering aftertreatment systems. Technical Report 2007–01–0318, SAE Technical Paper, 2007.

23. Wang Y, Kamp CJ, Wang Y et al. The origin, transport, and evolution of ash in engine particulate filters. *Applied Energy* 2020; 263: 114631.
24. Bai R and Tien C. Effect of deposition in deep-bed filtration: determination and search of rate parameters. *Journal of colloid and interface science* 2000; 231(2): 299–311.
25. Yamaguchi S, Fujii S, Kai R et al. Design optimization of wall flow type catalyzed cordierite particulate filter for heavy duty diesel. Technical report, SAE Technical Paper, 2005.
26. Tien C and Bai R. An assessment of the conventional cake filtration theory. *Chemical Engineering Science* 2003; 58(7): 1323–1336.
27. Tandon P, Heibel A, Whitmore J et al. Measurement and prediction of filtration efficiency evolution of soot loaded diesel particulate filters. *Chemical Engineering Science* 2010; 65(16): 4751–4760.
28. Lisi L, Landi G and Di Sarli V. The issue of soot-catalyst contact in regeneration of catalytic diesel particulate filters: A critical review. *Catalysts* 2020; 10(11): 1307.
29. Kuwahara T, Nishii S, Kuroki T et al. Complete regeneration characteristics of diesel particulate filter using ozone injection. *Applied energy* 2013; 111: 652–656.
30. Maunula T, Matilainen P, Louhelainen M et al. Catalyzed particulate filters for mobile diesel applications. Technical report, SAE Technical Paper, 2007.
31. Southward BW, Basso S and Pfeifer M. On the development of low pgm content direct soot combustion catalysts for diesel particulate filters. Technical report, SAE Technical Paper, 2010.
32. Yu M, Luss D and Balakotaiah V. Regeneration modes and peak temperatures in a diesel particulate filter. *Chemical engineering journal* 2013; 232: 541–554.
33. Viswanathan S, Rothamer D, Sakai S et al. Effect of particle size distribution on the deep-bed capture efficiency of an exhaust particulate filter. *Journal of Engineering for Gas Turbines and Power* 2015; 137(10).
34. Viswanathan S, Rothamer DA, Foster DE et al. Evolution of deep-bed filtration of engine exhaust particulates with trapped mass. *International Journal of Engine Research* 2017; 18(5-6): 543–559.
35. Torregrosa AJ, Broatch A, Bermúdez V et al. Experimental assessment of emission models used for ic engine exhaust noise prediction. *Experimental Thermal and Fluid Science* 2005; 30(2): 97–107.
36. Torregrosa AJ, Broatch A, García-Tíscar J et al. Experimental verification of hydrodynamic similarity in hot flows. *Experimental Thermal and Fluid Science* 2020; 119: 110220.
37. Torregrosa AJ, Serrano JR, Arnau FJ et al. A fluid dynamic model for unsteady compressible flow in wall-flow diesel particulate filters. *Energy* 2011; 36(1): 671–684.

38. Payri F, Desantes JM and Broatch A. Modified impulse method for the measurement of the frequency response of acoustic filters to weakly nonlinear transient excitations. *Journal of the Aoustical Society of America* 2000; 107(2): 731–738.
39. Morfey CL. Sound transmission and generation in ducts with flow. *Journal of Sound and Vibration* 1971; 14(1): 37–55.